The OMEGA instrument summary results.

Bibring J-P., Langevin Y., Altieri F., Arvidson R., Belluci G., Berthé M., S. Douté, Drossart P., T. Encrenaz, Forget F., Fouchet,T., Gendrin A., Gondet B., Mangold. N., Moroz V., Mustard J., Pinet P., Poulet F., Schmitt B., Sotin C., Soufflot A., Titov D., Zasova L., and the OMEGA team.

1. OMEGA instrument specifics

The Observatoire pour la Minéralogie, l'Eau, les Glaces et l'Activité (OMEGA) instrument on board MEx is a visible/near infrared hyperspectral imager, built under the responsibility of IAS (Institut d'Astrophysique Spatiale), Orsay, France (Principal Investigator, PI, and Project Manager, PM) and LESIA (Laboratoire d'Etudes Spatiales et d'Instrumentation en Astrophysique), Meudon, France, in cooperation with IFSI-INAF, Roma, Italy and IKI, Moscow, Russia (*Bibring et al.*, 2004a).

OMEGA couples an imaging capability, with an IFOV of 1.2 mrad, to a spectral capability, in acquiring for each pixel the spectrum from 0.35 to 5.1 µm, in 352 contiguous spectral channels ("spectels"), with a spectral sampling of 7 nm, 13 nm and 20 nm in the spectral ranges (0.35 to 1.0 µm), (0.93 µm to 2.65 µm), and (2.51 to 5.1 µm) respectively. OMEGA includes three spectrometers, one for the visible and near infrared "VNIR" range (0.35 to 1.0 µm), and two to cover the near-infrared "NIR" range from 0.93 to 5.1 µm. Two dedicated and co-aligned telescopes are used to illuminate VNIR and NIR channels separately. VNIR operates in the pushbroom mode; it images a given line of Mars, perpendicular to the drift velocity of the spacecraft, along one direction of a bi-dimensional CCD detector array, with the spectrum of each pixel spread over the other direction of the array by a concave holographic grating. The infrared channel operates in a whiskbroom mode: one pixel of Mars is imaged at a time, and its spectrum acquired on two IR linear arrays, from 0.93 µm to 2.65 µm ("SWIR", for "Short Wavelength IR") and from 2.51 to 5.1 µm ("LWIR", for "Long Wavelength IR") respectively. A scanning mirror ahead of the NIR telescope enables contiguous pixel imaging in the cross track direction, perpendicular to the spacecraft drift velocity. For VNIR, SWIR and LWIR, the second spatial dimension is provided by the movement of the spacecraft: along the time, three dimensional (two spatial and one spectral) image-cubes are built, which constitute the OMEGA data set.

The imaging performances can be summarized as follows: with an IFOV of 1.2 mrad, the spatial sampling (cross-track pixel size) is ~ 300 m when the observation is made close to periapsis, up to 4.8 km from an altitude of 4000 km. OMEGA prime goal is to perform a global coverage of Mars with a 1.5 - 4.8 km footprint, and to map selected areas amounting to ~ 5 % of the surface at high resolution (footprint < 400 m) – although the initial goal of the mission design was to acquire the global high resolution (100 m) coverage. The instrument design allows a total field of view of 128 pixels cross-track, or 8.8°, both for the VNIR pushbroom channel and the NIR whiskbroom one. However, the building of the images requires synchronizing the duration of a swath with the drift of the spacecraft in order to avoid both undersampling and oversampling. With an infrared integration time of typically 5 ms,

chosen to secure a SNR > 100, the swath varies from 16 pixels when acquired at periapsis (high spacecraft orbital velocity, ~ 4 km/s), to 128 pixels when operating above 1500 km (slower spacecraft drift, < 2 km/s). Thus the high resolution mode is made of strips some 5 to 8 km wide, and hundreds of km long, while the global coverage is made of strips 300 to 500 km in width, and thousands km in length.

The nominal pointing mode is nadir. In order to target given units of interest, nadir pointing with a constant cross-track offset angle must be implemented. In addition, some observations have been made in inertial mode (3 axis stabilized), in particular to acquire limb profiling, and in a “spot pointing”, or “EPF” (emission phase function) mode, to enhance the detection of atmospheric constituents. Due to severe mission resource constraints, mainly in energy and downlink capability, a strict sharing with other investigations was imposed by ESA, assigning OMEGA with an averaged data volume cap of 15%. This translated in OMEGA operating over less than one out of 4 orbits on the average, and for < 60 mn per orbit. As a consequence, a large number of specific targets were missed, and very little multiple coverage of the same area to monitor seasonal changes was performed, along the first 3 (terrestrial) years of operations.

2. Identification of atmospheric constituents

As it analyzes the solar radiation diffused by Mars, OMEGA spectral images always include signatures of the atmospheric constituents, both as gases and aerosols. Their retrieval is mandatory to identify surface features, and gives access to unique atmospheric properties, with the highest spatial sampling on board Mars Express (300 m from periapsis altitude). However, given the limited spectral sampling (7 to 20 nm), only the major (CO_2) and a few minor species (CO, H_2O and O_2) are unambiguously detected. Examples are given herebelow.

2.1. CO_2

An accurate radiative transfer model devoted to the retrieval of the three components (surface, gas, aerosols) is by essence complex and iterative. At first order, it is possible to independently calculate the atmospheric absorption. A dedicated model has been built for this purpose (*Melchiorri et al.,* 2006), which computes a multiplicative component in the synthetic spectrum representative of the main atmospheric contribution (CO_2, H_2O and CO) in the 1-2.7 µm range (corresponding to the SWIR-C channel). This model consists in a line-by-line spectroscopic calculation of the atmospheric absorption; a spectral atmospheric database is built for each OMEGA session, with a one-to-one correspondence. A priori knowledge of the atmospheric pressure is taken from the GCM predicted pressure (*Forget et al.*, 1999), as well as humidity factor and CO profile. Several spectra are calculated around the GCM-predicted position in parameter space, and a least-square fit adjustment is made to retrieve the observed atmospheric pressure. Each calculation is performed at the exact illumination and elevation conditions corresponding to the OMEGA observations.

The pressure measured in this way is not the actual Martian pressure, as at this stage no correction for dust opacity is performed: the “effective pressure” measured in the model is nevertheless correlated to the actual pressure, in a way that can be

constrained by a more sophisticated model, including the scattering which is developed as “second order” modelling (*Forget et al.,* 2007).

Since pressure variation on Mars are primarily correlated to the altitude of the surface, CO_2 being the dominant atmospheric compound, a first output of the model is an altimetry map along the OMEGA observations. This altimetry measurement can be checked against the MOLA measurement: effective pressure measurements are found to be accurate to 0.044 mbar (standard deviation), corresponding to an altimetry accuracy of 100 m (1σ). The instrumental noise itself is estimated to about 200 m. Therefore OMEGA atmospheric observation gives an altimetry measurement spatially better resolved than the a priori MOLA measurement, to an accuracy of a few hundred meters. This first step allows us to study pressure fluctuations beyond the altimetry variations: this second order study gives access to the search for global or local wave variations, at the 0.1 mbar pressure range, corresponding to the Martian meteorology. Similar searches have been tentatively made from Phobos/ISM observations (*Gendrin et al.,* 2003).

2.2. H_2O and CO variations

A second step in the study of atmospheric features from OMEGA observations is the H_2O and CO retrieval. Despite faint absorption at OMEGA resolution, the sensitivity of the instrument gives access to a good accuracy of the column density of these minor constituents. Study of spatial variations of the abundance ratio of H_2O and CO can therefore be made, after the correction for the altitude of the surface is performed. The 2.6 µm band of H_2O is used, and water vapour maps have been obtained, for Ls=94°-112°, corresponding to the sublimation of the northern hemisphere polar cap. A mixing ratio of H_2O in the range 2-3 10^{-4} is obtained at 40°N latitude, corresponding to 25 pr-µm, and 5-10 10^{-4} at 60-80°N, corresponding to 40-60 pr-µm. These results are consistent with previous MAWD/Viking and TES/MGS below 60°N (*Encrenaz et al.,* 2005).

CO abundance is measured with only a low accuracy, due to the low intensity of the (2-0) band at 2.3 µm. Nevertheless, spatial variations have been positively observed over Hellas at Ls=130°-150°, by a factor of 2 compared to Ls=330°-350° (*Encrenaz et al.*, 2006). This result is consistent with GCM predictions (*Forget et al.,* 2006), which indicate an enrichment of non-condensable species over Hellas during southern winter, due to local topography affecting the global circulation. Similar variations of argon have been observed on Hellas at similar Ls (*Sprague et al.,* 2004).

2.3. CO_2 fluorescence

Strong non-LTE emission of the Martian atmosphere is observed above the limb in the OMEGA observations in 3-axis stabilized mode. These emissions are identified to CO_2 at 4.3 µm, with a maximum at ~ 90 km altitude and CO at 4.7 µm with a peak emission at ~ 50 km. The CO_2 emission are at altitude well above any dust contamination, dust opacity reflection coming typically well below 60 km. Despite no direct observation of CO_2 emission in imaging mode has been made before Mars Express, the interpretation of these emission was well understood in advance from non-LTE modelling of the Martian atmosphere, with models developed in particular

for atmospheric profile accuracy measurements (*Lopez-Puertas et al.,* 1999). An example of a spectrum of fluorescence is given in Figure 2.1.a, the vertical variation of the integrated emission in the CO_2 and CO band being plotted in Figure 2.1.b. The main interest of OMEGA observation is to provide simultaneously the spectral information on CO_2, and an accurate imaging of the emission. For the first time, direct evaluation of the emissive altitudes can be obtained from the spectral images, and compared to the model. Improvement of the model has been provided to fit the data (*Drossart et al,* in preparation).

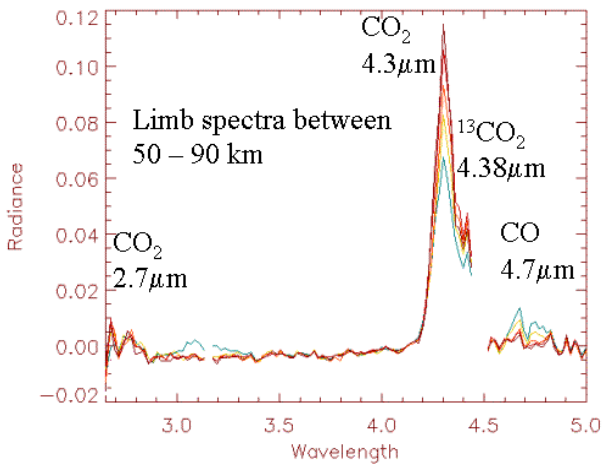

Figure 2.1.a: average of OMEGA spectra taken at the limb over altitudes in the range 50-90 km, exhibiting the fluorescence of CO_2 and CO in the atmosphere of Mars.

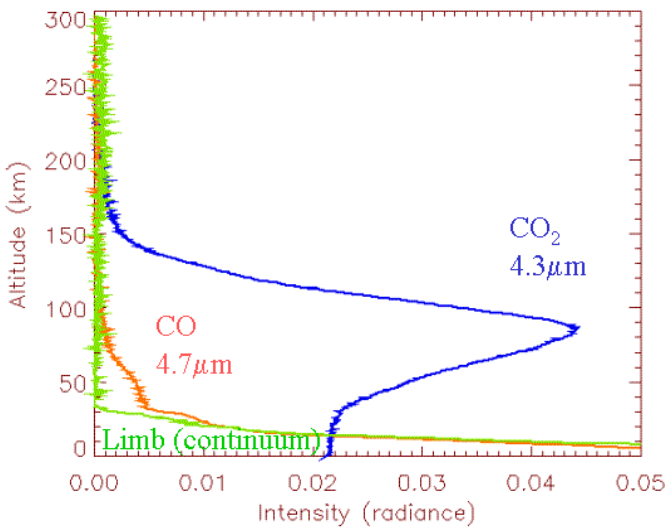

Figure 2.1.b: integrated emission on the spectral bands for CO_2, CO and the continuum, showing the maximum emission along the line of sight.

2.4. The O_2 dayglow

The O_2 emission at 1.27 µm was observed on the day side by OMEGA in both nadir and inertial modes of observation. In spite of the limited spectral sampling, it is possible to monitor the O_2 emission, as it does not overlap with emission or absorption features at a percent level. The O_2 dayglow at 1.27 µm is exited by the photolysis of ozone. About 90% of O_2 molecules are produced on the exited level $a^1\Delta_g$, which decays either by emitting 1.27 µm photons or by colliding with CO_2 molecules. From nadir observations, the distributions of the ozone abundances in latitude, local time and seasonal distributions are obtained: for the first time the signature of gravity waves in the O_2 emission, as well as CO_2 ice and H_2O ice clouds have been observed simultaneously in the Northern polar region at the end of winter. The OMEGA limb observations are used to determine the vertical distribution of the O_2 emission and the derived apparent ozone abundance, and to retrieve the vertical profile of the ozone number density. The O_2 emission profiles vary significantly with latitude, season and local time. Usually it is observed below 40 - 60 km. To estimate the vertical profile of the O_3 number density, the quenching effect was taken into account. From the limb profile of the O_2 emission, the quenching parameter was found to be k = (0.7 – 1) e^{-20} cm^3s^{-1}, which is about 2 - 3 times lower than the existing upper limit. To include into consideration the collisions of the O_2 with the CO_2 molecules, the vertical CO_2 profiles simultaneously obtained from the Mars Express/PFS LWC data were used. Below 10 km the aerosol absorption becomes significant even at low dust loading in the atmosphere, which obscures the O_2 emission. An example of the vertical profiles is given in Fig. 2.2.

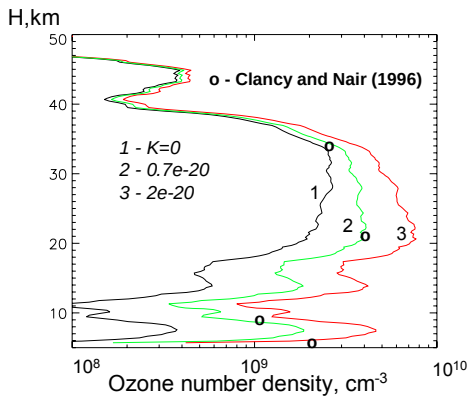

<u>Figure 2.2.</u>: vertical profile of ozone above Argire (44° S, 318° E) at Ls=16°, Lt=10.8h

3. Identification of surface constituents

In order to retrieve the diagnostic signatures of surface constituents, several steps are followed, and a variety of data reduction techniques are used. The first steps consist in removing the instrumental effects and the atmospheric contribution, dominated by the CO_2 bands (see above, 2.1.). Then, the spectrum is divided by a

synthetic solar reference one. The resulting radiance factor or I/F spectral values (where *I* is the measured radiance and πF is the incident solar radiance at the top of the martian atmosphere at the time of the observation) include all potential surface features.

Most features of interest can be enhanced by spectral band ratios, dividing the I/F at a wavelength position corresponding to the supposed maximum absorption (band center) to that of the nearby continuum. More sophisticated techniques are available, which for example search for coupled absorptions of a single component: the MGM (Modified Gaussian Model) is well suited to identify constituents exhibiting features that can be reproduced by a small number of Gaussian, such as pyroxene (see below, section 5).

4. OMEGA observations of frosts and ices

The OMEGA spectral characteristics and performances are very favorable for identifying H_2O and CO_2 ice and frost features in the SWIR channel, by the absorptions centered at (1.25 µm, 1.5 µm, 2 µm) and (1.435 µm, 2 µm) for H_2O and CO_2 respectively. Moreover, the band shapes (width and depth) are direct indicators of the texture and mean size of the icy grains, which enable their qualitative assessment (figure 4.1). Consequently, OMEGA has been able to monitor the seasonal evolution of both polar caps over one Martian year (*Bibring et al.*, 2005, *Langevin et al.*, 2005a, *Douté et al.*, 2006).

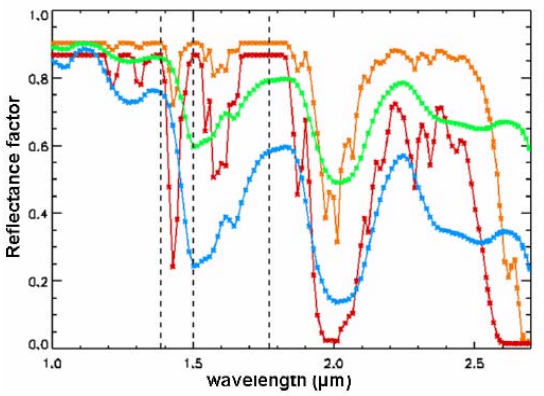

<u>Figure 4.1.:</u> model spectra of CO_2 ice with grains of 1 mm (orange) and 5 cm (red), and H_2O ice with grains sizes of 10 µm (green) and 1000 µm (blue). The three dashed lines correspond to the OMEGA spectels at 1.385 µm, 1.5 µm and 1.77 µm which are used for the determination of the strength of the H_2O ice absorption at 1.5 µm, as this is the only weak CO_2 absorption at these wavelengths.

Figure 4.2 illustrates the seasonal evolution of the North Polar cap. Condensation of both H_2O and CO_2 are roughly symmetrical in longitude, with H_2O frost observed down to 4° south of the CO_2 frost. When the sublimation is completed, all CO_2 disappears, leaving a pure H_2O-rich ice perennial cap.

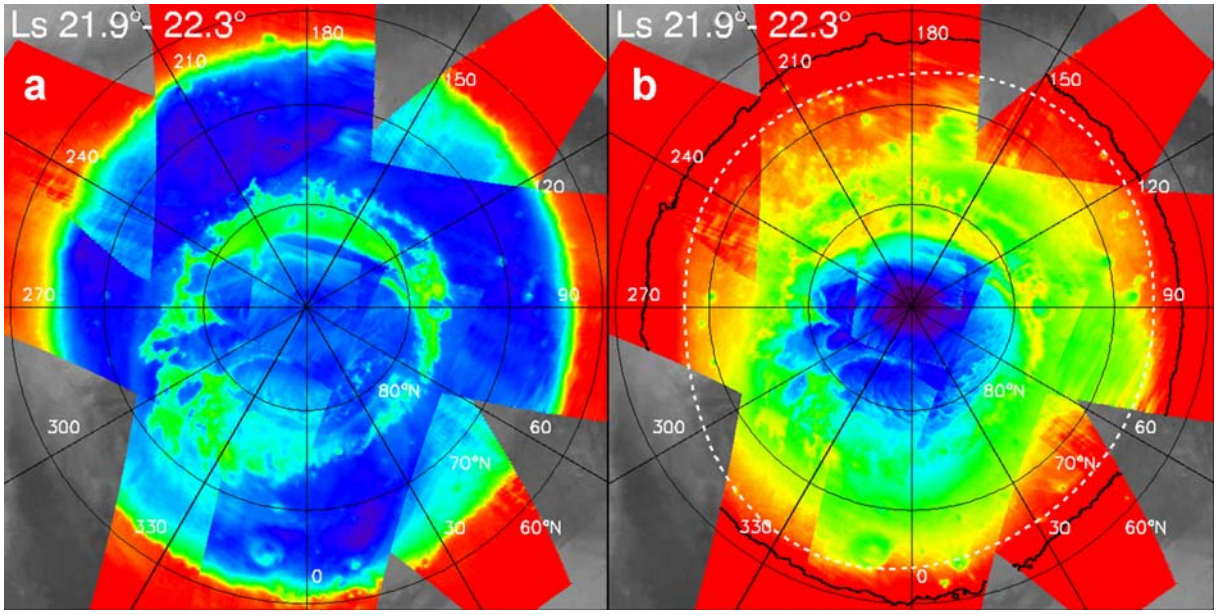

<u>Figure 4.2.</u>: seasonal evolution of the northern polar cap: spatial distribution of spectral signatures of H_2O ice and CO_2 ice observed by OMEGA in early northern spring (Ls 22°, March 2006). a) band depth of the H_2O ice absorption feature at 1.5 µm. The rainbow scale covers the range from 60% (black) to 0% (red); b) band depth of the CO_2 ice absorption feature at 1.43 µm, also from 60% (black) to 0% (red). The annulus observed by TES between the boundary of bright regions (black line on panel "b") and that of regions at the equilibrium temperature of CO_2 ice (crocus line, white dashes, from Titus and Kieffer, 2003) is confirmed as being constituted of H_2O frost. At this season, the strongest CO_2 ice signatures, corresponding to large mean grain sizes, are observed over regions corresponding to the central parts of the North permanent cap.

Previous observations in the visible (e.g. *Benson and James,* 2005) and in the thermal IR (*Kieffer et al.*, 2000) provided detailed information on the retreat of the southern seasonal cap. In mid spring, a cold and dark region (the “cryptic region”) develops over part of the cap (*Kieffer et al.*, 2000). The OMEGA observations have demonstrated that the Southern seasonal cap is almost free of water ice during most of the spring and summer, differing from the Northern seasonal cap. Furthermore, contrary to expectations, most of the cryptic region was shown to be dominated by dust contamination of the surface (*Langevin et al.*, 2006) with a possible link with a complex atmospheric circulation driven by the presence of Hellas basin.

The bright Southern perennial cap is constituted of a thin veneer of annealed CO_2 ice, containing trace amounts (~0.03 weight %) of dust and H_2O ice, probably trapped during the Southern winter (*Douté et al.,* 2006). It covers an extended H_2O-rich glacier (*Bibring et al.*, 2004b): the water ice, unambiguously identified by OMEGA, is mixed with dust and does not show up in visible images.

As a consequence, the two perennial caps constitute a major reservoir of the presently-known inventory of H_2O on Mars. Perennial CO_2 ice is apparently only a very minor constituent of the southern cap, and does not account for more than a small fraction of the present atmospheric mass of CO_2.

5. OMEGA observations of mafic minerals

The visible and near infrared spectral range has long been recognized as very favorable to identify diagnostic features of rock forming minerals, such as Fe electronic crystal field transitions in olivines and pyroxenes [e.g. *Adams and Filice,* 1967, *Soderblom*, 1992 and references herein]. Consequently, most olivine and pyroxene minerals can be identified from VNIR observations. Low-Fe silicates such as plagioclase feldspar, however, are nearly featureless in the VNIR and thus not readily identifiable with an instrument like OMEGA.

Pyroxenes [$(Ca,Fe,Mg)_2Si_2O_6$] are identified by the presence of two broad but distinct absorptions centered near 1 and 2 µm, with the band positions varying in a systematic pattern as a function of the pyroxene chemistry (Fe, Mg and Ca abundance) and crystal structure: the band centers shift towards longer wavelengths with increasing calcium content. Low calcium pyroxenes (LCP, e.g. orthopyroxene) have short wavelength band centers (~ 0.9 and ~ 1.85 µm) while high calcium pyroxenes (HCP, e.g. clinopyroxene) have their band centers at longer wavelength (1.05 and 2.3 µm). Because silicate rocks typical of terrestrial planet surfaces are mixtures of different minerals, the region around 1 µm can also exhibit absorption features that can originate from the presence of other minerals such as olivine (with a broad absorption centered at ~1.05 µm) and ferric oxides (with typical absorptions near ~0.9 µm). Most other minerals do not exhibit broad features near 2 µm, however. Therefore, it can be more definitive to detect pyroxenes through their ~2 µm features rather than their ~1 µm features.

We have defined a spectral index based on band ratios, enabling the detection of pyroxenes independent of their Ca content (*Poulet et al.*, 2007). The resulting maps of this mineral at a global scale reveal the contrast between the units having preserved their pristine mafic composition (the heavily cratered highlands crust and volcanic outflows), and large areas such as the northern plains which have apparently been altered to or covered by pyroxene-free materials. In parallel, we have developed an algorithm based on the MGM, well suited to identifying the pyroxene features, to discriminate between HCP and LCP and to weight their relative abundance (Figures 7.5.1. and 7.5.2.) (*Sunshine and Pieters*, 1993).

As a general trend, LCP is enriched in the older Noachian crust, while HCP is enriched in more recent lava flows (*Mustard et al.*, 2005). Figure 5.3 illustrates this pattern in the Syrtis major region (Nili Fossae / Nili Patera areas), where the volcanic shield exhibits the highest HCP/LCP abundance ratio found at Mars. HCP-rich areas are darker, and generally more sandy (Figure 5.4). The HCP enrichment of the lava outflows might indicate partial melting or a low level of mixing within the magma chamber, since HCP (*e.g.,* diopside) melts first, while LCP (*e.g.,* enstatite) requires higher temperatures to melt. By contrast, the Noachian crust appears to have crystallized out of a fully melted magma, mixing LCP and HCP.

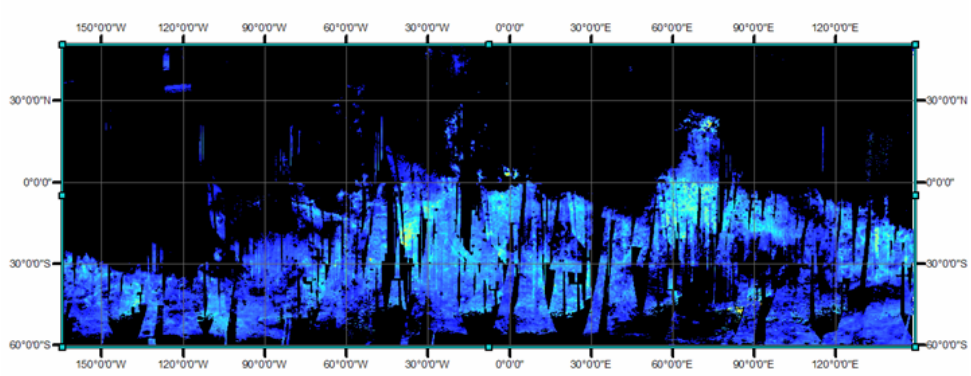

Figure 5.1.: OMEGA global mapping of Low Ca Pyroxene (LCP), for latitudes between -50° and + 50°.

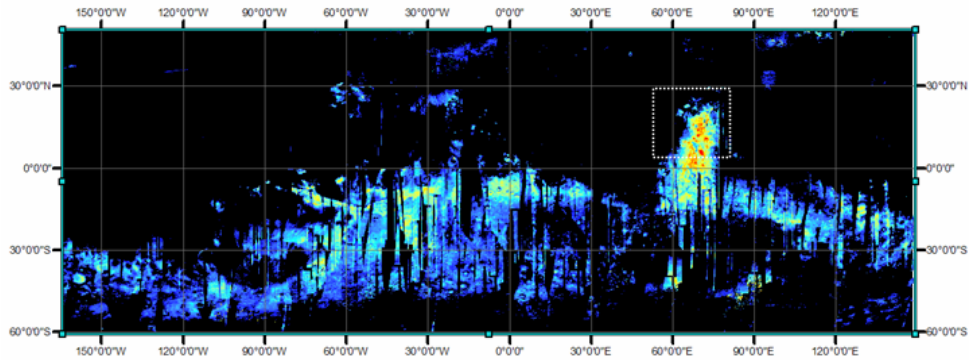

Figure 5.2.: OMEGA global mapping of High Ca Pyroxene (HCP), for latitudes between -50° and + 50°.

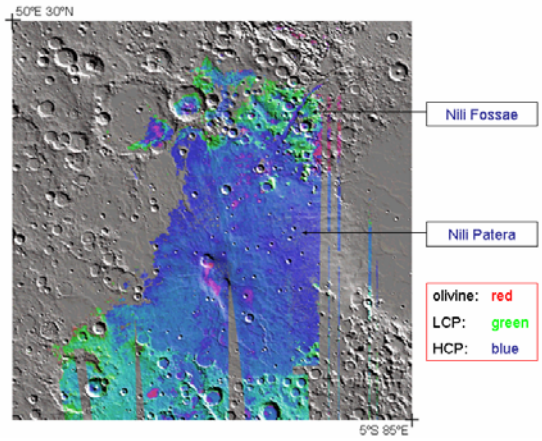

Figure 5.3.: OMEGA mineralogical mapping of the Syrtis Major area (square in fig. 5.2.), exhibiting the HCP rich lava outflows surrounded by the LCP rich Noachian crust and olivine rich spots.

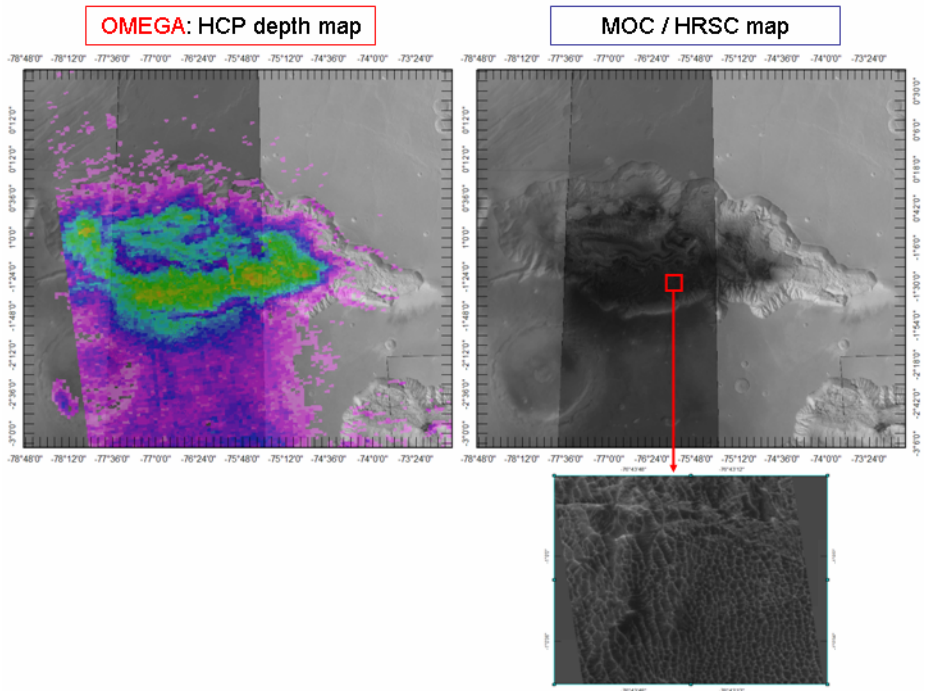

Figure 5.4.: mineralogical (OMEGA) and optical (MOC, HRSC) mapping of Hebes Chasma: HCP band depth (top left) is higher in the dark areas (top right), which appear as sand dunes (bottom right).

Olivine [$(Mg,Fe)_2SiO_4$] has a broad complex absorption centered near 1 µm, which extends from 0.8 to 1.5 µm; it broadens and deepens with increasing Fe content in the olivine, from forsterite Mg_2SiO_4 (Fo100) to fayalite Fe_2SiO_4 (Fo0) (*King and Ridley* 1987). For example, in USGS samples (*Clark et al.,* 1993), the absorption extends to about 1.55 µm for Fo89 and to 1.8 µm for Fo11. In addition, there are systematic variations in the shape of the 1 µm absorption with grain size: increasing the grain size broadens the bottom of the band and shifts the right wing towards longer wavelengths, so that forsterite with very large grains (> 100 µm) and fayalite with smaller grains have similar spectra. Therefore, a precise olivine composition in terms of Mg/Fe ratio is difficult to assess from NIR spectral data only. Olivine is primarily found in a variety of localized areas, including Nili Fossae and Terra Meridiani; in low albedo regions such as Aonia terra, Nereidum Montes, Terra Tyrrhena, Oenotria Scopulus; in several unnamed and named craters: Gale, Herschel, Huyghens, Schroeter, Pollack, Schiaparelli, Herschel, Moreux (figure 5.5); in Valles Marineris (Ius, Hebes, Capri, Melas, Ganges). A large number of isolated olivine-rich spots have been detected around the rims of Isidis, Hellas and Argyre (figure 5.6). In addition to these olivine-rich areas, detailed radiative transfer modeling (*Poulet et al.*, 2007) indicates that olivine is likely present together with pyroxene in the large mafic areas, mainly as forsterite of small grain sizes (< 10's µm), possibly with concentrations of up to 20%.

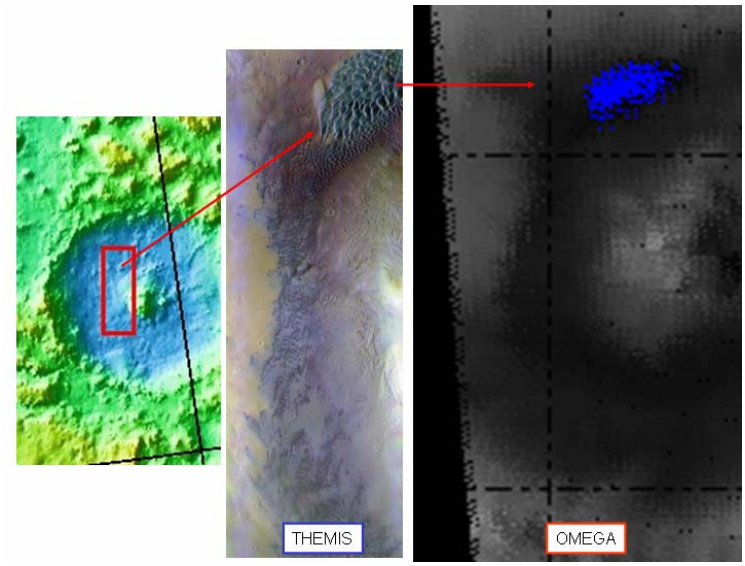

Figure 5.5.: olivine-rich dunes within Moreux crater, located at 41.5 N and 44.5 E, as identified by OMEGA (blue = olivine, right), in the MOLA (left) and THEMIS (middle) context.

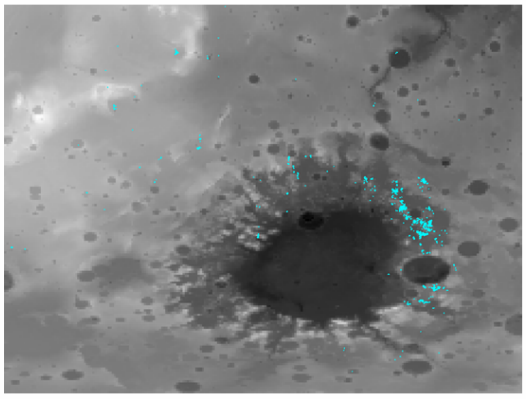

Figure 5.6.: olivine-rich spots surrounding the Argyre impact basin, centered at 50 S, 320 E), as identified by OMEGA (turquoise = olivine).

6. OMEGA observations of ferric oxides

Ferric-rich minerals can be detected through features in the visible and in the near infrared (e.g. *Burns,* 1993): the electronic transitions of ferrous iron, which lead to absorption band centers from 0.95 to 1.05 depending on the composition, shift towards smaller wavelengths (at ~ 0.85 to 0.9 µm) when the oxidation state varies from ferrous to ferric. In addition, the spectrum of ferric-rich phases exhibits some specific features in the visible, with in particular a shallow absorption at ~ 0.6 µm with

an edge at ~ 0.53 µm. Several indexes have thus been defined to identify ferric minerals. However, they do not lead to identical maps, which indicates that the surface of Mars contains a variety of ferric minerals that differ in composition, structure, crystallinity, and/or mean grain size, and therefore may record possibly distinct formation processes.

The index based on the 0.53 µm absorption edge integrates all ferric-rich phases [*Bell et al.,* 1990; *Morris et al.,* 2000]. The corresponding ferric mineral map (figure 6.1.b) shows a positive detection all over the martian surface, with a high variation in intensity, well correlated to the near infrared albedo (measured at 1.1 µm) (figure 6.1.a). Smaller concentrations are detected in the low albedo mafic units, which could correspond to the presence of ferric minerals in the bulk of the crust.

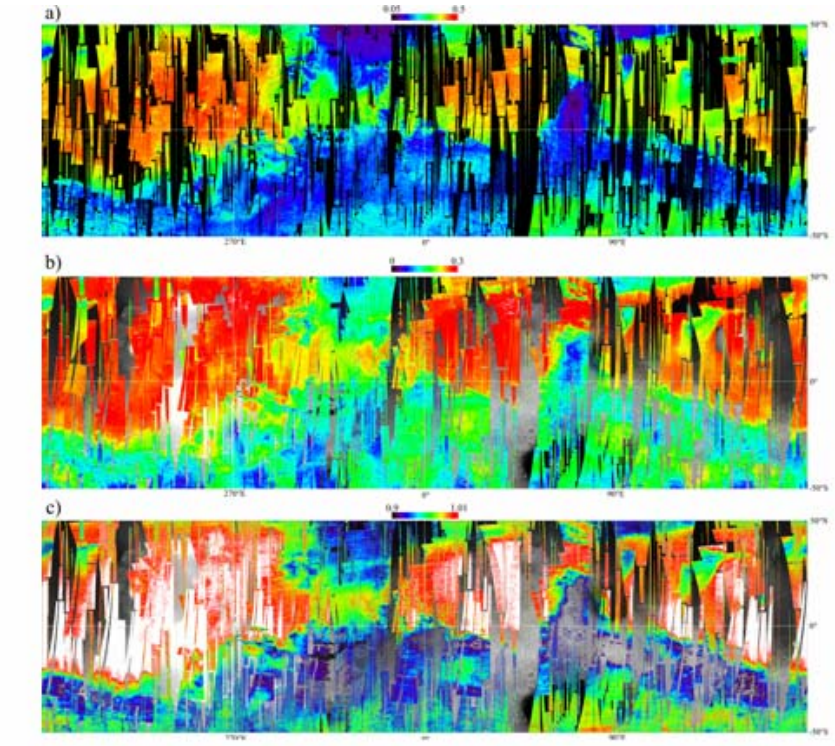

Figure 6.1.: global maps of (a) the NIR albedo; (b) ferric oxides, and (c) nanophase ferric oxides.

Higher concentrations of ferric minerals are found in the vast areas which do not exhibit mafic signature: they may result from the alteration of these mafic regions, and appear as a bright reddish soil ("dust"). These areas correspond also to a positive detection when another spectral index, ratioing the reflectance at 0.98 and 0.8 µm, is used. This index is sensitive to the presence of so-called nanophase hematite (nanometer-sized particles of α-Fe_2O_3), as shown by *Morris et al.*, 2000 (figure 6.1.c). The dust is subjected to atmospheric transport, resulting in the coverage of wide areas such as Olympus Mons and Tharsis volcanoes. However, this mobility does not affect the entire Mars surface, as demonstrated by the high mineralogical diversity still observed at all resolutions. An important observation made by OMEGA is that these ferric oxides, as shown hereafter (7.), are strictly anhydrous. On this basis, the OMEGA team has proposed that they result from an alteration by atmospheric peroxides rather than by liquid water (*Bibring et al.*, 2006).

A third and distinct class of ferric phases is detected by the occurrence of a deep 0.9 µm band and a strong reflectance increase to 1.3 µm (figure 6.2.). Such features are located in a few areas only, and appear coupled to the presence of hydrated minerals, mostly sulfates. This class of ferric phases has been found in Terra Meridiani, Aram Chaos, and in association with layered deposits in Valles Marineris (figure 6.3.).

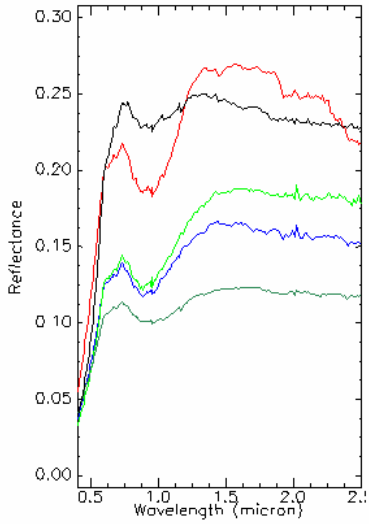

Figure 6.2.: typical OMEGA spectra of oxide-rich areas: Aram Chaos (red), Candor Chasma (green), Capri Chasma (blue), compared to that of dust (black).

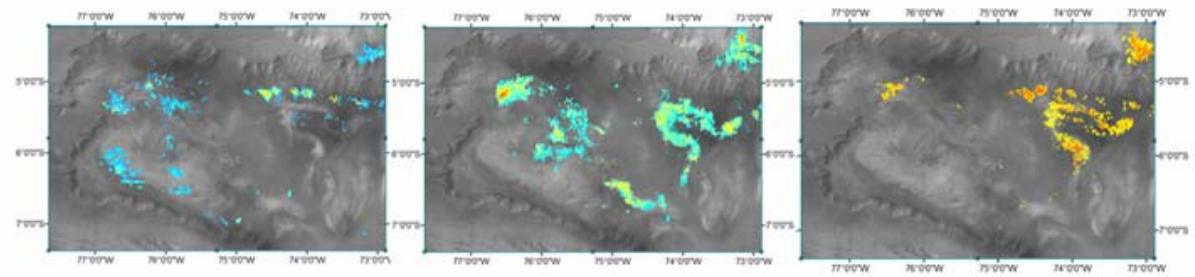

Figure 6.3.: spatial coupling of sulfates and oxides in Candor Chasma. Left: 1.9 µm band depth identified as polyhydrated sulfates (blue = 2%, red = 5% and above). Middle: 2.1 µm band depth, identified as kieserite (green = 2%, red = 5% and above). Right: oxide band depth, as modeled using the MGM of Sunshine and Pieters (1993) (orange = 10%, red = 30% and above).

7. OMEGA detections of hydrated minerals

Minerals with water molecules either adsorbed or in their crystal structure exhibit relatively well-defined absorptions near 1.4 µm, 1.9 µm and 3.0 µm, and are thus readily accessible to OMEGA detection. O-H stretching, either symmetric (v_1) or asymmetric (v_3), has its fundamental absorption band at 2.9 µm, with overtones and

combinations at 1.4 µm ($v_1 + v_3$). The H-O-H bending fundamental at ~ 6 µm (v_2) has its first overtone at 3.1 µm, and a combined resulting feature ($v_2 + v_3$) at ~ 1.9 µm. These near-IR features have been studied previously in lower spatial and spectral resolution Mars data sets (*e.g.,* Houck *et al.*, 1973; Pimentel *et al.,* 1974; Calvin, 1997).

All hydrated phases do exhibit a broad 3 µm band, which is thus not diagnostic of specific minerals. However, it can be used to evaluate the amount of water stored in the mineral structure (*Jouglet et al.*, 2007, *Milliken et al.*, 2007). Hydrated minerals are thus identified by features resulting from O-H and/or H_2O related vibrations, at ~ 1.4 µm and ~ 1.9 µm, together with those resulting from the coupling between OH and/or H_2O to metal (e.g. Al, Mg, Fe, Ca) or to anionic complexes such as SO_4^{2-}, CO_3^{2-} (*e.g., Clark et al.* 1990*a,b*; *Swayze and Clark* 1990). Minerals containing hydroxyls exhibit the 1.4 µm band, as well as narrow absorptions between 2.0 to 2.4 µm which are typically combination overtones of an OH stretch and a metal-OH bend, and can be very diagnostic of mineralogy (*e.g., Bishop et al.* 1993, 1994; *Roush et al.*, 1993; *Bell et al.,* 1994). Hydrated sulfates have specific features resulting from the S-O stretches (fundamentals at ~ 10 µm), with overtones in the 2.2 - 2.5 µm region when in presence of water (*e.g.*, *Crowley* 1991; *Cloutis et al.,* 2006). Their precise position and shape of the sulfate near-IR bands vary with composition, and for hydrated sulfates result in features at 2.2 and 2.4 µm. An important exception is that of monohydrated sulfate (e.g. kieserite $MgSO_4$, H_2O), for which the 1.4 µm and 1.9 µm bands are shifted towards longer wavelengths, at 1.6 µm and 2.1 µm respectively.

OMEGA has identified and mapped two classes of hydrated minerals: sulfates (section 7.1) and phyllosilicates (section 7.2). By contrast, carbonates (7.3), which have two strong absorptions features at ~3.5 and ~3.9 µm, have not been detected so far, above the detection limit of ~1-2% in volume, demonstrated by ground calibration.

One key outcome of OMEGA detection of hydrated species is that they are found in only very localized areas (fig. 7.1). In particular, the ferric oxides that constitute the bright dust, which covers most of the northern plains and Tharsis, are strictly anhydrous (see above 6).

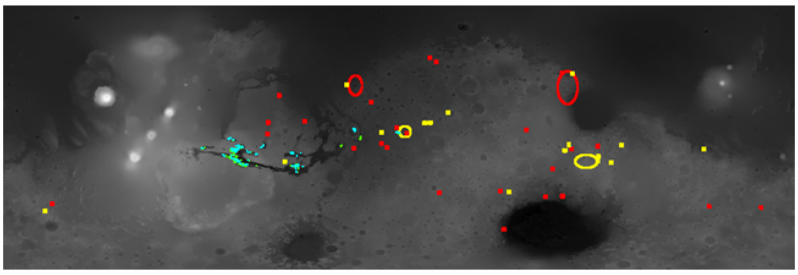

Figure 7.1.: distribution of hydrated minerals detected so far by OMEGA at the surface of Mars, for latitude from - 50° to + 50°. Blue: kieserite; green: polyhydrated sulfates; red: phyllosilicates; yellow: other hydrated minerals.

7.1. Hydrated Sulfates

Hydrated sulfates have been detected by OMEGA at the surface of Mars in three locations: in layered deposits of Valles Marineris (*Gendrin et al.*, 2005), in Terra Meridiani (*Arvidson et al.*, 2005) and in dark dunes of the Northern polar cap *(Langevin et al.*, 2005b). In most cases, mixtures of sulfates are present. In a few cases however, due to their diagnostic signatures, specific sulfates have been identified with a high level of confidence: kieserite ($MgSO_4$, H_2O) and gypsum ($CaSO_4$, 2 H_2O).

Gypsum exhibits in its 1.2 µm to 2.6 µm spectrum six unique spectral features, at 1.45 µm, 1.75 µm, 1.94 µm, 2.22 µm, 2,26 µm and 2.48 µm, which makes its potential for identification quite robust (figure 7.2). OMEGA could at the same time *(Langevin et al.*, 2005a): i) identify H_2O as the dominant constituent of the permanent (residual) Northern cap, exclusive of CO_2 ice, ii) map its spatial distribution, and iii) identify gypsum as the major constituent of the dark terrains of Olympia Planitia intermixed with the bright ice (figure 7.3).

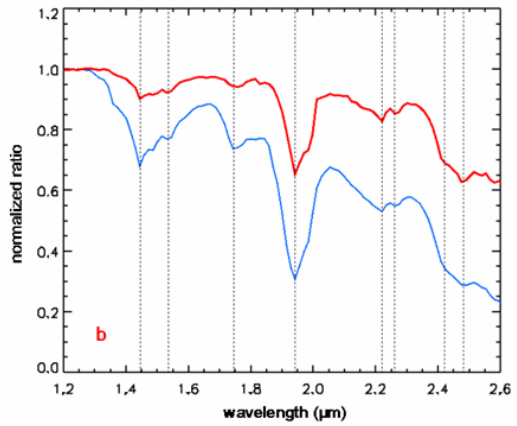

<u>Figure 7.2.</u>: red curve: OMEGA spectrum from 1.2 µm to 2.6 µm of a sulfate rich region within the dark dunes of Olympia Planitia, within the northern polar cap, ratioed to a reference spectrum of a close-by dark area, normalized to 1 at 1.25 µm; blue curve: normalized ratio of two spectra obtained during ground calibration, that of a pure gypsum powder (< 40 µm grain size) and that of an aluminum oxide powder, which is spectrally featureless in this wavelength range. Features are observed in both spectral ratios at 1.445 µm, 1.535 µm, 1.745 µm, 1.94 µm, 2.22 µm, 2.26 µm, 2.42 µm and 2.48 µm (dashed lines).

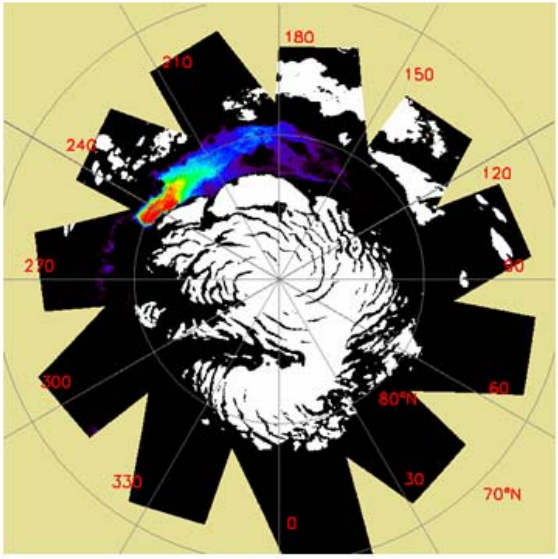

<u>Figure 7.3.</u>: area interpreted to be gypsum rich within Olympia Planitia, illustrated by a false color composite showing the distribution of the absorption at 1.93 µm relative to a continuum defined from 1.86 µm and 2.14 µm. The color code is a rainbow scale from black (< 4% band depth) through blue, green and yellow to red (> 25% band depth). A strong absorption at 1.93 µm is observed on an extended dark area centered at 240° E, 80° N. White areas correspond to the regions with permanent water ice at the surface.

Kieserite also has specific features in terms of position and shapes, at 1.6 µm, 2.1 µm and 2.4 µm (figure 7.4). Its presence in a few locations at the surface of Mars is important as this monohydrated mineral is known to be easily hydrated into epsomite ($MgSO_4$, $7H_2O$) which can eventually dehydrate to hexahydrite ($MgSO_4$, $6H_2O$) and amorphous Mg sulfate ($MgSO_4$, $1.2H_2O$). Kieserite has been identified in several layered deposits within Valles Marineris (figure 7.5), as well as in a small spot north East of the Mars Exploration Rover (MER) Opportunity landing site, in Terra Meridiani (figure 7.6).

Most of hydrated sulfates detected by OMEGA appear to be polyhydrated, including possibly the amorphous Mg sulfate phase. *Poulet et al.*, 2007 have shown that some of the sulfates detected in Terra Meridiani could be Fe-rich sulfates, for example amarantite $(Fe^{3+})(SO_4)(OH)\cdot 3(H_2O)$ or schwertmannite $(Fe^{3+}{}_{16}O_{16}(OH)_{12}(SO_4)_2\cdot nH_20)$; however jarosite $((K,Na,H_3O)Fe_3(SO_4)_2(OH)_6)$, detected by Opportunity, has a specific NIR spectrum which is not observed in OMEGA data.

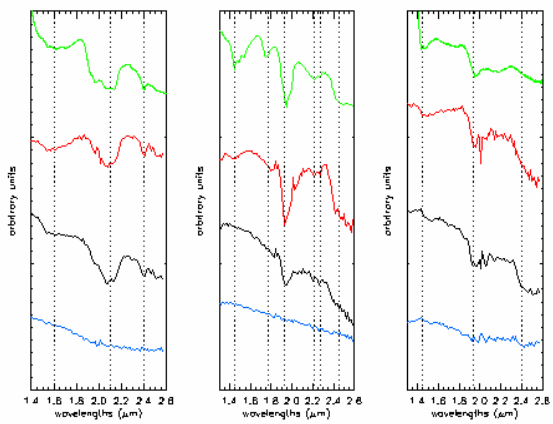

Figure 7.4.: hydrated sulfate spectra identified in the OMEGA observations. Green: library spectrum. Black: OMEGA spectrum. Blue: reference spectrum. Red: spectral ratio. Left: kieserite ($MgSO_4$, H_2O). Middle: gypsum ($CaSO_4$, $2H_2O$). Right: polyhydrated sulfate; the library spectrum corresponds to epsomite ($MgSO_4$, $7H_2O$) but other polyhydrated sulfates are good spectral analogues.

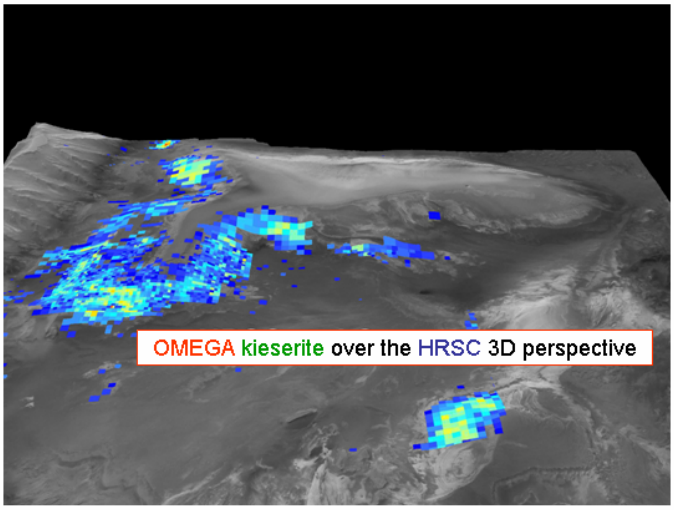

Figure 7.5.: spatial distribution of the kieserite, identified in OMEGA spectra, plotted over the HRSC 3D perspective model of Candor Chasma.

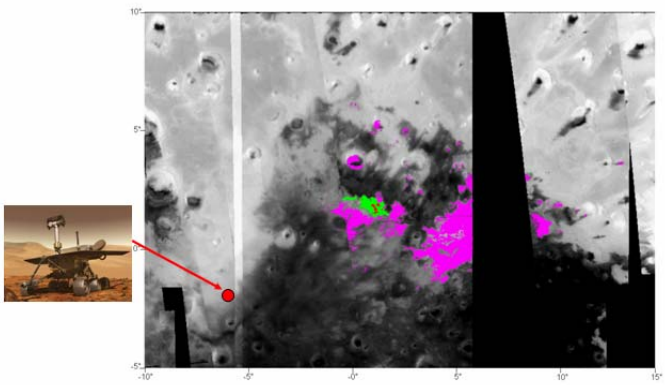

Figure 7.6.: distribution of kieserite (red), polyhydrated sulfates (green) and other hydrated minerals (pink) in Terra Meridiani. Opportunity site is shown.

7.2. Hydrated phyllosilicates

As shown in figure 7.1, OMEGA has detected a variety of phyllosilicates in localized areas, with the two largest ones located in the Nili Fossae and Mawrth Vallis areas (*Poulet et al.*, 2005). These detections constitute the best evidence that Mars once hosted liquid water over long durations, to enable the formation of these hydrated alteration phases.

The composition of the phyllosilicates is not identical in all locations (figure 7.7). Mg/Fe smectites are always present, in particular as nontronite, and dominate in the Nili Fossae / Syrtis Major complex. Al-rich phyllosilicates, such as montmorillonite or chlorite, are also found, in particular in the Marwth Vallis area. However, kaolinite appears to be rare. This is an indication that the process responsible for the formation of the phyllosilicates, although it implies liquid water over long durations, was characterized by a rather low level of leaching (*Chevrier et al.*, 2007). With reference to conditions prevailing in terrestrial environments or during laboratory simulations when similar minerals are formed, the martian fluids in which these smectites formed were neutral to alkaline rather than acidic at the time the aqueous alteration took place (*Chevrier et al.*, 2007).

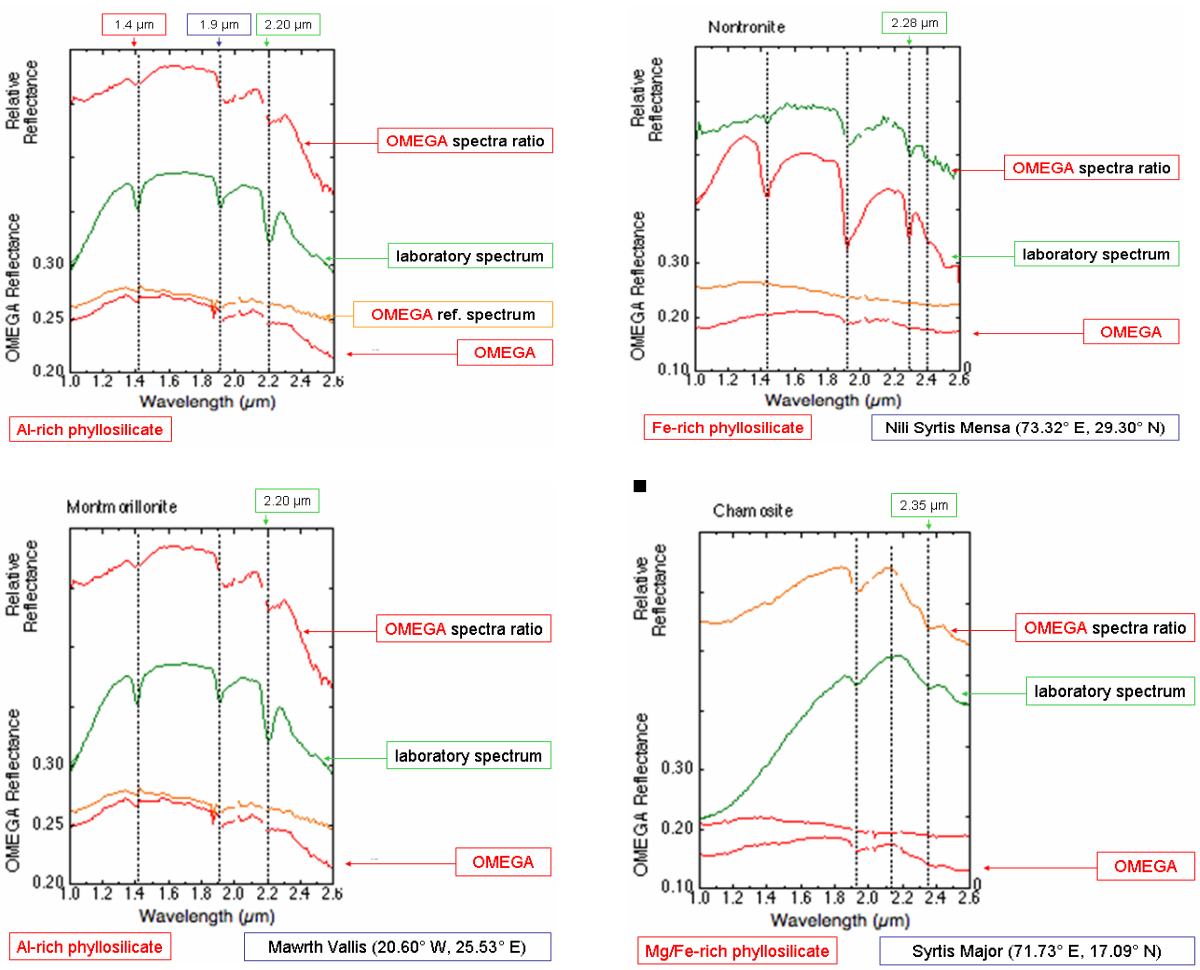

<u>Figure 7.7.</u>: spectra of hydrated phyllosilicates, as detected by OMEGA, compared to laboratory spectra, showing the diagnostic shift of the M-OH feature from 2.2 µm for Al-rich (a,b) to 2.28 µm Fe-rich (c) and 2.35 µm Mg/Fe-rich (d) species.

The sites in which the phyllosilicates are mapped are all very ancient, exposed to the surface either by impact or erosion. In the Nili Fossae area (*Mustard et al.*, 2007, *Mangold et al.*, 2007), the phyllosilicate-rich terrains all appear to predate the first lava flows from Nili Patera and Syrtis Major Planum, dated early Hesperian by crater counting. Phyllosilicate-rich sites include both ancient heavily crated terrains, which have not been buried by the lava flows, and recently excavated ones (Figure 7.8): apparently the impact process did not destroy or dehydrate these minerals, but might rather have triggered their formation. It is important to note that by contrast, the lobate ejecta craters within the Nili Patera lava floor do not exhibit hydrated minerals, which strongly indicates that this lava material was essentially dry.

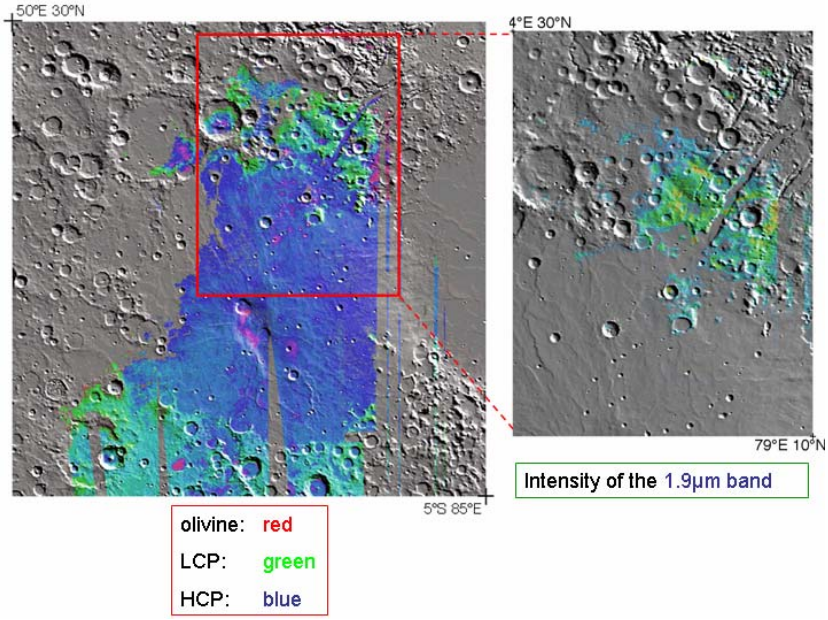

Figure 7.8.: hydrated phyllosilicates in Nili Fossae. The intensity of the 1.93 µm feature (right) indicates the location of the hydrated clays, found in the ancient terrains not buried by lava flows.

In Mawrth Vallis (*Poulet et al.*, 2005, *Loizeau et al.*, 2007), as in all similar outflow channels, no hydrated minerals are found within the bed or the mouth of the channel (figure 7.9.). In contrast, hydrated minerals are found on the highly etched terrains along the flanks of the channel. One interpretation of this observation is that the phyllosilicates were formed prior to the outflow. The outflows themselves do not appear to have lasted long enough, nor constituted a sustained enough degree of fluvial activity, to form hydrated minerals such as clays. Rather, the outflow channels may result from transient episodes (e.g. *Baker et al,* 1974), violent enough to erode their flanks and expose ancient materials which happen to have been processed by liquid water, in earlier times. Those earlier phyllosilicates then remained preserved as such until today.

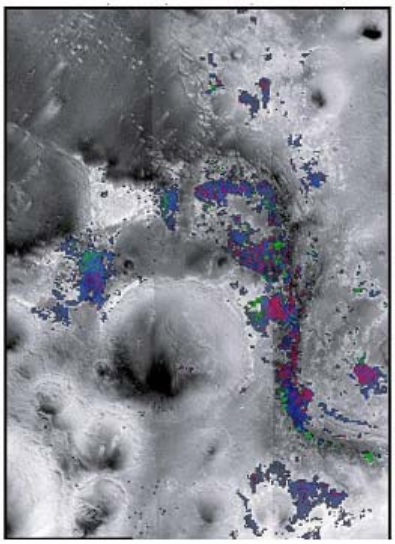

Figure 7.9.: hydrated phylloslicates in Mawrth Vallis. Distribution, over an HRSC mosaic (3 contiguous maps), of the minerals identified by OMEGA through their 1.93 µm (hydration, blue), 2.20 µm (montmorillonite, green) and 2.30 µm (Mg/Fe rich smectites, red) features.

7.3. Hydrated carbonates, and other CO_2 sinks

We have searched the OMEGA data for carbonates in a wide variety of potential sites, all over the planet. In particular, we have performed a systematic characterization of the material related to impact craters within the northern plains, with the following rationale: if Mars once hosted a large ocean at a time when the atmosphere was dense enough for CO_2 to dissolve, ionize and precipitate (as on the Earth) sedimentary layers of hydrated carbonates might have accumulated on the hypothetical ocean floor prior to these low altitude terrains draining, drying out, and filling with lava. Large enough impact craters could have reached down into these older layers and exposed in their ejecta some of their constitutive material. In fact, in their OMEGA spectra, most craters with diameter larger than ~ 20 km exhibit a clear signature of the crustal (mafic) bedrock (*Bibring et al.*, 2005). However, none of the ejecta, nor the central peaks, show the spectral signature of carbonates, nor even of any hydrated minerals. This is a strong indication that these terrains probably never hosted long-standing water bodies in the presence of a dense CO_2-rich atmosphere.

As described above (section 4), OMEGA has shown that the two perennial polar caps are massive water ice glaciers, but do not constitute significant CO_2 traps. With the lack of detection of abundant carbonates, it seems very likely that the atmosphere, although extremely tenuous, is the dominant CO_2 reservoir at present. This constitutes a major constraint in describing the long term climatic evolution of Mars.

8. A derived Mars mineralogical history: identification and characterization of an early Mars global change.

The identification and mapping of both primary igneous and secondary altered minerals, put into their geomorphological context, reveals some major features relevant to Mars history (*Bibring et al.*, 2006). Well preserved mafic minerals are still observed, on a wide scale, in the oldest crust and, in places, even in impact craters. By contrast, the northern lowlands are dominated by an alteration product (dust) characterized by anhydrous ferric oxide. Hydrated minerals have been detected, in a restricted number of localized areas. They consist of two classes, phyllosilicates and sulfates, which are found in distinct terrains, formed by distinct processes, at distinct times: they trace distinct eras, “phyllosian” and “theiikian” respectively to reflect the name, in greek, of their dominant minerals. Stratigraphic relationships suggests that the phyllosilicates have formed first, in a neutral to alkaline environment, followed by the sulfates (theiikos in greek), in an acidic environment. We are thus led to propose that in between the two eras, Mars underwent a global-scale climatic change. We attribute this major environmental evolution to the volcanic activity that led to the building of Tharsis and the filling of the northern plains (figure 8.1).

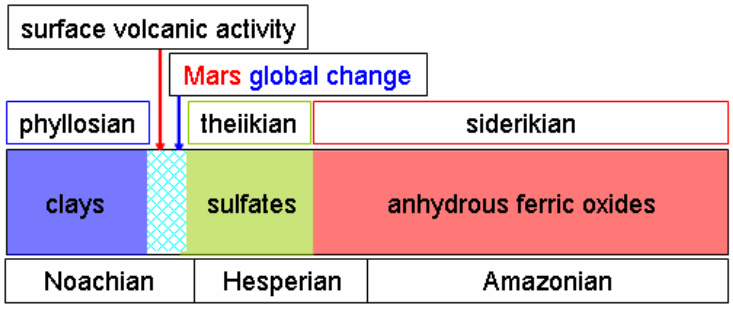

Figure 8.1.: OMEGA derived Mars mineralogical History

Since phyllosilicates usually require water over long duration to form, Mars likely hosted conditions sustaining liquid water on geological timescales in its very early history. This in turn requires there to have been abundant greenhouse gases, given the predicted low luminosity of the early Sun (*e.g., Pollack et al.,* 1987). However, like most young stars, the early Sun was likely an extreme ultraviolet emitter, with high ionizing efficiency, and with an intense solar wind: a planetary magnetic shield was thus critical to protect against atmospheric loss. As demonstrated by the findings of remnant crustal magnetism by MAG/ER investigation on Mars Global Surveyor, early Mars appears to have supported a global dynamo, which could have efficiently protected its atmosphere. The absence of magnetized minerals over Tharsis and in the northern plains is a strong indication that this dynamo shut off before the onset of volcanism that raised Tharsis and filled the plains.

A possible explanation is that mantle convection could not sustain a sufficient temperature difference between the core and the mantle, required to maintain core convection: the dynamo and its associated magnetic shield dropped. Cold plumes could have started to form and to sink within the mantle and accumulate at the

core/mantle boundary. This, in turn, could have triggered thermal instabilities, leading to the formation of degree 1 hot plumes, ascending to form Tharsis after some tens of millions years. In such a scheme, the formation of Tharsis would have happened long after the magnetic field had faded, and long after most of the atmosphere had been lost by solar wind erosion or other processes. In the tenuous resulting atmosphere, the massive outgassing coupled to the volcanic activity could have injected S-rich compounds as dominant species, which then rapidly oxidized into sulfuric compounds, leading the environment (including any groundwater) to become highly acidic. These S-rich species precipitated widely over the planet, possibly in the form of nanophase S-rich grains, possibly accounting for the large concentration of S detected by elemental APXS analyses at all rover and lander sites since Viking.

.

The present composition of martian atmosphere has an N_2/CO_2 value close to both the Venus value and that of the Earth (~ 3 %), if one takes into account that most of the initial terrestrial CO_2 is presently trapped as carbonates. The N_2/CO_2 ratio is consistent with such an early physical loss mechanism. If the initial volatile reservoirs of Mars, Venus and the Earth were similar, and given that CO_2 can be sequestered into carbonates whereas N_2 hardly ever condenses into minerals, one would not expect a massive depletion of both constituents (more than 99.9 %) with an identical efficiency. OMEGA data support a model in which most of the atmosphere escaped prior to the Theiikian; today's atmosphere would result from an equilibrium between the present (very limited) loss mechanisms, for example as measured by Mars Express/ASPERA (*Barabash et al.*, 2007), and the supply of volatiles by residual internal activity.

In such a model, the Phyllosian era would have ended when the surface water could no longer remain stable as a liquid, instead evaporating and/or percolating and freezing as subsurface permafrost. The large scale tectonic effects that followed the building of Tharsis, such as the opening of Valles Marineris and the tilt of Terra Meridiani, as well as the localized rising of the geothermal water table, could have produced sequential supplies of liquid water to a variety of regions within these areas, for example cementing the S-rich nanophase grains into large sulfate deposits. This process would not necessarily require surface liquid water to be long-lasting, since sulfates can sediment even while water is evaporating. During this period, sulfate layers would have grown where surface water was supplied, in spatial and time relation with the Tharsis rise. The Theiikian era would have ended rapidly, leading to a long era (Siderikian), lasting until the present, dominated by anhydrous surface oxidation and the creation of nanophase ferric oxides (siderikos in Greek) in a highly rarefied atmosphere. This oxidation likely results from a very slow process (time scales of Gy) operating on the very superficial layers (sub-mm scale) of surface grains.

9. Summary.

Although one could have expected that the global circulation of dust would preclude identifying distinct units at the surface of Mars, the OMEGA investigation demonstrates a high degree of mineralogical diversity down to a subkilometre scale. Units of all ages, from the most ancient, to the most recently processed ones, have been identified by their composition. In particular, the oldest units, although subjected to a longer period of potential weathering, still preserve their igneous content. In

parallel, the detection and mapping of alteration products give key clues to decipher the evolution of the Mars environment. Two classes of hydrated phases have been identified: placed in their geological context, and in relation with the *in situ* findings of the two NASA/MERs, they enable a profoundly new model of the past martian climate to be envisioned. Thirty years after the pioneering measurements of the Viking landers, the OMEGA orbital near infrared survey indicates that Mars might indeed have hosted, once in its earlier past, conditions favoring liquid water to remain stable over long periods of time. The sites in which one might search for these potential habitats are not necessarily located where the optical images would have led us to consider, since phyllosilicates are not directly associated with fluvial or other water-related lanforms. OMEGA results so far suggest that the most favorable sites for preserving evidence of this early epoch are those that are characterized by a mineralogical signature of hydrated phyllosilicates. Most of the largest of these targets may have already been identified. A refined analysis by the Compact Reconnaissance Imaging Spectrometer for Mars instrument on the just-begun Mars Reconnaissance Orbiter mission, with similar spectral coverage but a ten-fold higher spatial sampling than OMEGA, will greatly enhance the characterization of these regions. It is our deep conviction that if ever life once emerged on Mars, these phyllosilicate-rich sites are the targets in which future *in situ* laboratories (for example the NASA Mars Science Laboratory and ESA/ExoMars missions) have the best chances of finding potential biorelics, at a microscopic scale.

References

J.B. Adams and A.L. Filice, Spectral reflectance 0.4 to 2.0 microns of silicate rock powders, *J. Geophys. Res.* 72, 5705-5715, 1967

R.E. Arvidson, F. Poulet, J-P. Bibring, M. Wolff, A. Gendrin, R.V. Morris, J.J. Freeman, Y. Langevin, N. Mangold, G. Bellucci, Spectral Reflectance and Morphological Correlations in Eastern Terra Meridiani, Mars, *Science* 307, 1591-1594, 2005

V.R. Baker and D.J. Milton, Erosion by catastrophic floods on Mars and Earth, *Icarus* 23, 27-41, 1974

S. Barabash, A. Fedorov, R. Lundin and J-A. Sauvaud, Martian Atmospheric Erosion Rates, *Science* 315, 501-503, 2007

J.F. Bell, T.B. McCord, P.D. Owensby, Observational evidence of crystalline iron oxides on Mars, *J. Geophys. Res.* 95, 14447-14461, 1990

J.F. Bell III, J.B. Pollack, T.R. Geballe, D.P. Cruikshank, and R. Freedman, Spectroscopy of Mars from 2.04 to 2.44 μm during the 1993 opposition: Absolute calibration and atmospheric vs. mineralogic origin of narrow absorption features, *Icarus, 111,* 106-123, 1994.

J.L. Benson and P. B. James, Yearly comparisons of the Martian polar caps: 1999-2003 Mars Orbiter Camera observations, *Icarus*,174, 513-523, 2005

J-P. Bibring and S. Erard, The Martian Surface, *Space Science Reviews* Vol. 96, Nos 1-4, 293-316, 2001

J-P. Bibring, A. Soufflot, M. Berthé, Y. Langevin, P. Drossart, M. Bouyé, M. Combes, P. Puget, A. Semery, G. Bellucci, V. Formisano, V. Moroz, V. Kottsov, OMEGA : Observatoire pour la Minéralogie, l'Eau, les Glaces et l'Activité, *ESA SP* 1240, 37-49, 2004a

J-P. Bibring, Y. Langevin, F. Poulet, A. Gendrin, B. Gondet, M. Berthé, A. Soufflot, P. Drossart, M. Combes, G. Bellucci, V. Moroz, N. Mangold, Perennial water ice identified in the south polar cap of Mars, *Nature* 428, 627-630, 2004b

J-P. Bibring, Y. Langevin, A. Gendrin, B. Gondet, F. Poulet, M. Berthé, A. Soufflot, R.E. Arvidson, N. Mangold, J.F. Mustard, P. Drossart, Mars surface diversity as revealed by the OMEGA/Mars Express Observations, *Science* 307, 1591-1594, 2005

J-P. Bibring, Y. Langevin, J.F. Mustard, F. Poulet, R.E. Arvidson, A. Gendrin, B. Gondet, N. Mangold, P. Pinet, F. Forget, Global Mineralogical and Aqueous Mars History Derived from OMEGA/Mars Express Data, *Science* 312, 400-404, 2006

J.L. Bishop, C.M. Pieters and R.G. Burns 1993. Reflectance and Mössbauer spectroscopy of ferrihydrite-montmorillonite assemblages as Mars soil analog materials. *Geochim. Cosmochim. Acta* 57, 4583-4595.

J.L. Bishop, C.M. Pieters, and J.O. Edwards 1994. Infrared spectroscopic analyses on the nature of water in montmorillonite. *Clays and Clay Minerals*, 42, 6, 702-716.

R.G. Burns, *Mineralogical Applications of Crystal Field Theory,* Cambridge University Press , 1993

W.M. Calvin, 1997. Variation of the 3-□m absorption features on Mars: Observations over eastern Valles Marineris by the Mariner 6 infrared spectrometer. *J. Geophys. Res.* 1002 E4, 9097-9107.

V. Chevrier, F. Poulet a,d J-P. Bibring, Early geochemical environment of Mars as determined from thermodynamics of phyllosilicates, submitted to *Nature*, 2007

A. Chicarro, P. Martin, R. Trautner, The Mars Express Mission: an Overview, *ESA SP* 1240, 3-13, 2004

R.N. Clark, T.V.V. King, M. Klejwa, G.A. Swayze, and N. Vergo 1990*b.* High spectral resolution reflectance spectroscopy of minerals. *J. Geophys. Res.* 95, 12653-12680.

R.N. Clark, G.A. Swayze, A. Gallagher, T.V.V. King, W.M. Calvin, The USGS, Digital Spectral Library: Version 1: 0.2 to 3.0 µm, USGS, *Open File Report 93-592*, 1993

J.K. Crowley 1991. Visible and near-infrared (0.4-2.5 µm) reflectance spectra of playa evaporite minerals. *J. Geophys. Res.* 96, 16,231-16,240.

E.A. Cloutis, F.C. Hawthorne, S.A. Mertzman, K. Krenn, M.A. Craig, D. Marcino, M. Methot, J. Strong, J.F. Mustard, D.L. Blaney, J.F. Bell III, and F. Vilas, Detection and discrimination of sulfate minerals using reflectance spectroscopy, *Icarus, 184,* 121-157, 2006.

S. Douté, B. Schmitt, Y. Langevin, J-P. Bibring, F. Altieri, G. Bellucci, B. Gondet, F. Poulet, South Pole of mars: Nature and Composition of the Icy terrains from Mars Express OMEGA Observations, Plan. Space Science, 2006

T. Encrenaz, R. Melchiorri, T. Fouchet, P. Drossart, E. Lellouch, B. Gondet, J-P. Bibring, Y. Langevin, D. Titov, N. Ignatiev, F. Forget, A mapping of martian water sublimation during early northern summer using OMEGA/Mars, *Astronomy and Astrophysics,* 441, Issue 3, October III 2005, L9-L12, 2005

T. Encrenaz, T. Fouchet, R. Melchiorri, P. Drossart, B. Gondet, Y. Langevin, J-P. Bibring, F. Forget, B. Bézard, Seasonal variations of the Martian CO over Hellas as observed by OMEGA/Mars Express, *Astronomy and Astrophysics,* 459, Issue 1, November III 2006, 265-270, 2006

F. Forget, F. Hourdin, R. Fournier, C. Hourdin, O. Talagrand, M. Collins, S.R. Lewis, P.L. Read, J-P. Huot, Improved general circulation models of the Martian atmosphere from the surface to above 80 km, *J. Geophys. Res.,* 104, Issue E10, 24155-24176, 1999

A. Gendrin, S. Erard, P. Drossart, R. Melchiorri, Observation of pressure variations in the Martian atmosphere, *Geophysical Research Letters,* 30, Issue 23, pp. ASC 14-1, 2003

A. Gendrin, N. Mangold, J-P. Bibring, Y. Langevin, B. Gondet, F. Poulet, G. Bonello, C. Quantin, J.F. Mustard, R.E. Arvidson, S. LeMouelic, Sulfates in Martian layered terrains : the OMEGA/Mars Express View, *Science* 307, 1587-1591, 2005

J.R. Houck, J.B. Pollack, C. Sagan, D. Schaack, and J.A. Decker Jr 1973. High Altitude Infrared Spectroscopic Evidence for Bound Water on Mars. *Icarus* 18, 470.

D. Jouglet, F. Poulet, R.E. Milliken, J.F. Mustard, J-P. Bibring, Y. Langevin, B. Gondet, Hydration state of the Martian surface as seen by Mars Express OMEGA I: Analysis of the 3 µm feature, *J. Geophys. Res.* 2007

H.H. Kieffer, T. N. Titus, K. F. Mullins, P. R. Christensen, Mars South polar spring and summer behavior observed by TES: Seasonal cap evolution controlled by frost grain size, *J. Geophys. Res.*, 105, 9653-9700, 2000

T.V.V. King and W.I. Ridley, Relation of the Spectroscopic Reflectance of Olivine to Mineral Chemistry and Some Remote Sensing Implications, *J. Geophys. Res.* 92, 11457-11469, 1987

Y. Langevin, F. Poulet, J-P. Bibring, B. Schmitt, S. Douté, B. Gondet, Summer Evolution of the North Polar Cap of Mars as Observed by the OMEGA/Mars Express Observations, *Science* 307, 1581-1584, 2005a

Y. Langevin, F. Poulet, J-P. Bibring, B. Gondet, Sulfates in the North Polar Region of Mars Detected by the OMEGA/Mars Express Observations, *Science* 307, 1584-1586, 2005b

Y. Langevin, S. Douté, M. Vincendon, F. Poulet, J-P. Bibring, B. Gondet, B. Schmitt, F. Forget, No signature of clear CO2 ice from the "cryptic" regions in Mars ' south seasonal polar cap, *Nature* 442, 831-835, 2006

D. Loizeau, N. Mangold, F. Poulet, J-P. Bibring, A. Gendrin, V. Ansan, C. Gomez, Y. Langevin, B. Gondet, P. Masson, G. Neukum, Phyllosilicates in the Mawrth Vallis region of Mars, *J. Geophys. Res.*, 2007

M. A. López-Valverde, D.P. Edwards, M. López-Puertas, C. Roldán, Non-local thermodynamic equilibrium in general circulation models of the Martian atmosphere 1. Effects of the local thermodynamic equilibrium approximation on thermal cooling and solar heating, *J. Geophys. Res.,* 103, Issue E7, 16799-16812, 1998

N. Mangold, F. Poulet, J.F. Mustard, J-P. Bibring, B. Gondet, Y. Langevin, V. Ansan, P. Masson, C. Fassett, J.W. Head, H. Hoffmann, G. Neukum, Mineralogy of the Nili Fossae region with OMEGA/MEx dara : 2. Aqueous alteration of the crust, *J. Geophys. Res.*, 2007

R. Melchiorri, P. Drossart, T. Fouchet, B. Bézard, F. Forget, A. Gendrin, J-P. Bibring, N. Manaud, and the OMEGA Team, A simulation of the OMEGA/Mars Express observations: Analysis of the atmospheric contribution, *Planet. and Space Science,* 54, 774-783,(2006

R.E. Milliken, J.F. Mustard, F. Poulet, D. Jouglet, J-P. Bibring, B. Gondet, Y. Langevin, Hydration state of the Martian surface as seen by Mars Express OMEGA II: H2O content of the surface, *J. Geophys. Res.* 2007

R.V. Morris, D.C. Golden, J.F. Bell, T.D. Shelfer, A.C. Scheinost, N.W. Hinman, G. Furniss, S.A. Mertzman, J.L. Bishop, D.W. Ming, C.C. Allen, D.T. Britt, Mineralogy, composition, and alteration of Mars Pathfinder rocks and soils: Evidence from multispectral, elemental, and magnetic data on terrestrial analogue, SNC meteorite, and Pathfinder samples, *J. Geophys. Res.*, 105, E1, 1757-1818, 2000

J.F. Mustard, F. Poulet, A. Gendrin, J-P. Bibring, Y. Langevin, B. Gondet, N. Mangold, G. Bellucci, F. Altieri, Olivine and Pyroxene Diversity in the Crust of Mars, *Science* 307, 1594-1597, 2005

J.F. Mustard, F. Poulet, J.W. Head, N. Mangold, J-P. Bibring, S.M. Perkey, C. Fassett, Y. Langevin, G. Neukum, Mineralogy of the Nili Fossae region with OMEGA/MEx dara : 1. Ancient Impact LMelt in the Isidis basin and Implication for the Transition from the Noachian to Hesperian, *J. Geophys. Res.*, 2007

G.C. Pimentel, P.B. Forney, K.C. Herr 1974. Evidence about hydrate and solid water in the Martian surface from the 1969 Mariner infrared spectrometer. *J. Geophys. Res.* 79, 1623-1634.

J.B. Pollack, J.F. Kasting, S.M. Richardson, and K. Poliakoff, The case for a wet, warm climate on Mars, *Icarus, 71,* 203-224, 1987.

F. Poulet, C. Gomez, J-P. Bibring, Y. Langevin, B. Gondet, P. Pinet, G. Bellucci, J.F. Mustard, Martian Surface Mineralogy from OMEGA/MEx: Global mineral maps, *J. Geophys. Res.*, 2007

F. Poulet, J. P. Bibring, J. F. Mustard, A. Gendrin, N. Mangold, Y. Langevin, R. E., Arvidson, B. Gondet, C. Gomez, Phyllosilicates on Mars and implications for early martian climate, *Nature* 438, 623-628, 2005

T.L. Roush, D.L. Blaney, and R.B. Singer 1993. The surface composition of Mars as inferred from spectroscopic observations. In *Remote Geochemical Analysis: Elemental and Mineralogical Composition* (C.M. Pieters and P.A.J. Englert, Eds.), pp. 367-393, Cambridge University Press, Cambridge, UK.

L. Soderblom, The Composition and Mineralogy of the Martian Surface from Spectroscopic Observations : 0.3 µm to 50 µm, in H. Kieffer, B. Jakovsky, C. Snyder and M. Matthews eds., *Mars*, Univ. Arizona Press, Tucson, 557-597,1992

A.L. Sprague, W.V. Boynton, K.E. Kerry, D.M. Janes, D.M. Hunten, K.J. Kim, R.C. Reedy, A.E. Metzger, Mars' South Polar Ar Enhancement: A Tracer for South Polar Seasonal Meridional Mixing, Science, 306, 1364-1367, 2004

J.M. Sunshine and C. M. Pieters, Estimating modal abundances from the spectra of natural and laboratory pyroxene mixtures using the modified Gaussian model, J. Geophys. Res., 98, 9075?9087, 1993

G.A. Swayze, and R.N. Clark 1990. Infrared spectra and crystal chemistry of scapolites: Implications for Martian mineralogy. *J. Geophys. Res.* 95, 14481-14495.

T.N. Titus, and H. H. Kieffer, A comparison of the Mars south polar recession rates between 1999 and 2001, *Lunar Planet. Sci. Conf.* 33, 2071, 2002